Anthropocene xxx (xxxx) xxx–xxx

Contents lists available at ScienceDirect

Anthropocene

journal homepage: www.elsevier.com/locate/ancene

Agricultural land use doubled sediment loads in western China's rivers

Amanda H. Schmidt[a,*], Veronica Sosa Gonzalez[b], Paul R. Bierman[b], Thomas B. Neilson[b], Dylan H. Rood[c,d,e]

[a] Geology Department, Oberlin College, Oberlin, OH, USA
[b] Geology Department and Rubenstein School of the Environment and Natural Resources, University of Vermont, Burlington, VT, USA
[c] Department of Earth Science and Engineering, Imperial College London, South Kensington Campus, London SW7 2AZ, UK
[d] Accelerator Mass Spectrometry Laboratory, Scottish Universities Environmental Research Centre, East Kilbride G75 0QF, UK
[e] Earth Research Institute, University of California, Santa Barbara, CA 93016, USA

ARTICLE INFO

Keywords:
Be-10
Sediment generation
Sediment yield
Erosion index

ABSTRACT

Land use changes, such as deforestation and agricultural expansion, increase soil erosion on the scale of hillslopes and small drainage basins. However, the effects of these changes on the sediment load in rivers is poorly quantified, with a few studies scattered globally, and only 10 data points in the world's most populous nation, China. At 20 different sites in western China, we compare contemporary fluvial sediment yield data collected daily over 4 to 26 years between 1945 and 1987 (median = 19 years) to long-term measures of sediment generation based on new isotopic measurements of *in situ* ^{10}Be (beryllium-10) in river sediments. We find that median sediment yield at these sites exceeds background sediment generation rates by a factor of two (from 0.13 to 5.79 times, median 1.85 times) and that contemporary sediment yield is statistically significantly different from long-term sediment generation rates ($p < 0.05$). Agricultural land use is directly and significantly proportional to the ratio of contemporary sediment yield to long term sediment generation rates (Spearman correlation coefficient rho = 0.52, $p < 0.05$). We support these findings by calculating erosion indices, which compare the delivery of meteoric ^{10}Be to each watershed with the export of meteoric ^{10}Be bound to riverine sediment. Erosion indices are also directly and significantly proportional to agricultural land use (rho = 0.58, $p < 0.05$). Together, these data sets suggest that upstream agricultural land use has significantly increased sediment supply to rivers in western China, likely increasing turbidity and decreasing ecosystem services such as fisheries.

1. Introduction

The local effects of deforestation and conventional agriculture on erosion, soil productivity (Matson et al., 1997; Montgomery, 2007), river ecosystems (Gellis et al., 2017), and the global carbon budget (Lal, 2003) include erosion of soil faster than it forms (Amundson et al., 2015). Comparing long-term rates of sediment generation with current rates of sediment export (yield) quantifies how land use changes affect watersheds. Better understanding of human effects on erosion, sediment transport, and sediment yield has implications for ecosystem services in river environments, including habitat for aquatic animals (Gellis et al., 2017), sedimentation of reservoirs (Wang et al., 2005), and nutrient supply to rivers through nutrients adsorbed to sediment (Walling et al., 2003).

Direct comparisons of short-term sediment yield to long-term sediment generation rates are limited (Covault et al., 2013). Covault et al.'s (2013) compilation and several subsequent studies (Bartley et al., 2015; Chappell et al., 2006; Reusser et al., 2015; Schmidt et al., 2011; Vanacker et al., 2014) compare background sediment generation rates to contemporary gauging station data from 16 studies of sediment yield, of which three were in Europe, five in the United States, two in the South America, one in Australia, and the remaining five in Asia. The Asian studies include data from Taiwan (n = 1) (Dadson et al., 2005; Siame et al., 2011), Sri Lanka (n = 9) (Hewawasam et al., 2003), Israel (n = 1) (Clapp et al., 2000), and China. The China studies focus on tributaries to the Yangtze River (n = 5) (Chappell et al., 2006) and Yunnan and Tibet (n = 5) (Schmidt et al., 2011), but these 10 data points cover only the steep headwater reaches of the rivers draining the region, which have relatively little agriculture.

With thousands of years of human history, the effect of long-term agricultural land use on sediment supply to rivers in China provides valuable data on how humans have altered sediment fluxes on the planet. In this paper, we quantify the landscape-scale effect of long-term agricultural land use in China by comparing the sediment yield in

* Corresponding author.
E-mail address: aschmidt@oberlin.edu (A.H. Schmidt).

http://dx.doi.org/10.1016/j.ancene.2017.10.002
Received 30 May 2017; Received in revised form 12 October 2017; Accepted 17 October 2017

20 rivers (basin area, 31–213,260 km^2; median = 5640 km^2) to background rates of sediment generation determined using measurements of *in situ* produced ^{10}Be (beryllium-10) in river sediment (Bierman and Steig, 1996; Brown et al., 1995; Granger et al., 1996). The sediment analyzed for ^{10}Be was collected at or near the gauging stations used to quantify sediment yield (Fig. 2). In addition, because we also measured meteoric ^{10}Be for each sample, we are able to provide the first large-scale follow up of the erosion index method proposed by Brown et al. (1988) as a measure of isotopic steady state in a watershed. These data are important because meteoric ^{10}Be can be measured in any sample, regardless of quartz content of the upstream watershed, making it a potentially powerful tool for assessing human impacts on the environment across a wide range of lithologies.

2. Background

In situ-produced ^{10}Be (^{10}Be$_i$), measured in fluvial sediment, has been used extensively to quantify rates of erosion and infer background rates of sediment generation mostly, but not exclusively, in small, headwater basins. ^{10}Be$_i$ concentration in sediment is inversely related to erosion rate (Bierman and Steig, 1996; Brown et al., 1995; Granger et al., 1996) and erosion and sediment generation rates calculated from measured ^{10}Be$_i$ concentration are insensitive to human activities, as long as erosion does not exceed the depth of the mixed soil layer (~100 cm) (Bierman and Steig, 1996; Brown et al., 1995; Granger et al., 1996; Reusser et al., 2015; Schmidt et al., 2016; Vanacker et al., 2007; Von Blanckenburg et al., 2004).

Meteoric ^{10}Be (^{10}Be$_m$) forms in the atmosphere through cosmic-ray induced spallation of nitrogen and oxygen (Lal and Peters, 1967). Once formed, the isotope adheres to aerosols and is delivered to Earth's surface by either precipitation or dry deposition (Graly et al., 2011; Willenbring and von Blanckenburg, 2010). The delivery of ^{10}Be$_m$ is a function of latitude, precipitation rate, and the movement of the isotope within the atmosphere (Graly et al., 2011; Willenbring and von Blanckenburg, 2010). When considered along with contemporary sediment yield data, ^{10}Be$_m$ can be used to calculate the erosion index (EI) of a watershed, which reflects the balance between atmospheric delivery and fluvial export of the isotope; the erosion index is a function of erosion intensity and sediment transport efficiency (Brown et al., 1988). Brown et al. (1988) found that higher erosion indices were associated with landscapes with more human disturbance upstream of the sample site, but this approach has not been applied beyond the basins Brown studied (primarily in the southeastern United States with a global compilation of 11 continent-scale watersheds as well).

The degree to which chemical weathering (dissolution) is included in erosion rates measured with ^{10}Be$_i$ varies depending on the depth of the weathering front in the study area (Fig. 1). If the weathering front is shallow (< 2 m below the surface), then most ^{10}Be$_i$ production will co-occur with solution weathering and erosion rates calculated with ^{10}Be$_i$ will include mass loss both through solution and physical transport. However, if the weathering front is deeper than the 2 m penetration depth for neutrons producing most ^{10}Be$_i$, then erosion rates calculated with ^{10}Be$_i$ will reflect primarily physical processes of mass loss (erosion) and thus underestimate total mass lost from the system.

Prior comparisons of contemporary sediment yield with long term sediment generation rates determined by ^{10}Be$_i$ measurements in detrital sediment come to one of four conclusions: 1) the landscape is in mass steady state (Matmon et al., 2003; Wittmann et al., 2011), i.e., has similar background rates of sediment generation and short-term sediment yield; 2) dams have reduced contemporary sediment yield (Syvitski et al., 2005) or raised apparent ^{10}Be$_i$-derived sediment generation rates (Reusser et al., 2017); 3) stochastic, high-magnitude, low-frequency events not well captured by contemporary sediment yield records increase background sediment generation (Covault et al., 2013; Kirchner et al., 2001; Schaller et al., 2001; Schaller et al., 2001); or 4) land use change has increased contemporary sediment yield (Hewawasam et al., 2003; Reusser et al., 2015), at least in the smallest watersheds (Vanmaercke et al., 2015). With the exception of 10 data points (Chappell et al., 2006; Schmidt et al., 2011), these studies have not focused on China, despite China's large population and long history of intensive human land use.

One major source of uncertainty in these studies is that many rely solely on suspended sediment measurements to estimate contemporary sediment yield. Suspended sediment is only part of the sediment moved out of a system in rivers and relying just on suspended sediment measures without considering bedload (Fig. 1), as many studies do (e.g., Clapp et al., 2000; Hewawasam et al., 2003; Kirchner et al., 2001; Reusser et al., 2015), means that contemporary sediment yield is underestimated. Some studies have bedload data and include these in measures of contemporary sediment yield (e.g., Schaller et al., 2001; Vanacker et al., 2014), while other studies apply a correction factor that increases sediment yield by an estimate of bedloads for the studied rivers (e.g., Bartley et al., 2015). Dissolved load is important when considering total mass loss from the system but unlike bedload is not directly relevant to the comparison between suspended load and cosmogenically determined rates of denudation except when substantial chemical weathering and solution loss occurs in the upper 2 meters. In that case, cosmogenic erosion rates should exceed rates of sediment transport.

3. Study site

Our study focuses on rivers draining from the Tibetan Plateau through Yunnan province, China. Due to the thousands of years of agricultural land use in the area and the long record of Chinese gauging station data (Schmidt et al., 2011), this region is ideal for testing whether land use alters the rate at which rivers export sediment. Our sampling locations are on larger rivers in the northern parts of the study area and on smaller rivers in the southern parts. The sampling scheme reflects the location of sediment gauging stations (Schmidt et al., 2011).

The geology of the eastern Tibetan Plateau and Yunnan and the resulting landscape are diverse and formed as a result of the India-Asia collision and the outward expansion of the Tibetan Plateau (Burchfiel and Chen, 2012). Our study area includes the sedimentary Qiangtang and Lhasa Terranes in the Tibetan Plateau headwaters of the Salween and Mekong, and the sedimentary redbeds of the Lanping Simao, the slightly metamorphosed sedimentary and volcanic Baoshan, and Chengling-Mengliang terranes to the south (Akciz et al., 2008; Burchfiel and Chen, 2012). In addition, the Gaoligong Shan, Chongshan, Xuelong Shan, and Ailao Shan shear zones all run through the study area (Akciz et al., 2008; Burchfiel and Chen, 2012).

The topography of our study area is as varied as the geology (Figures DR1). We sampled watersheds in the Salween, Mekong, Red, and Irrawaddy catchments. Basins range in size from 7 km^2 to 189,000 km^2 (basin area and topography data from NASA LP-DAAC (2012)). Mean basin elevations range from < 1400 to > 4600 m; mean basin slopes range from 14° to 23° for a moving window 90 m^2 in size. The largest basins we sampled are on the Yangtze, Mekong, and Salween Rivers; these sites are sampled in their respective gorges and have relatively steep average basin slopes (≥20°) and large upstream areas (≥88,000 km^2). South in the study area and away from the margins of the Tibetan Plateau, average basin slopes generally decrease (Figure DR1).

Study area climate is monsoonal and dominated by interaction between the East Asian summer monsoon and the Indian summer monsoon, as well as by topography (Yatagai et al., 2012). Sampled basins receive between 500 and 1400 mm of precipitation annually (Figure DR1) (Yatagai et al., 2012). During the monsoon season (June to September), 85% of the annual precipitation falls and the rivers transport 62% of the annual discharge and 86% of their annual suspended sediment load (Henck et al., 2010). Soil erosion is intensified during the monsoon months by flooding and runoff (Yang et al., 2010). Broadly

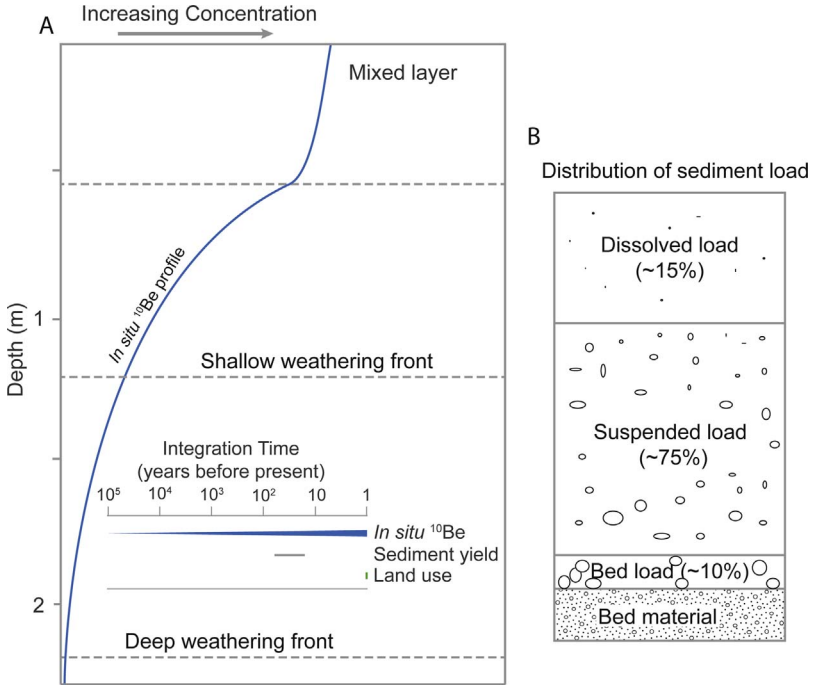

Fig. 1. (A) Conceptual figure showing how the depth of the weathering front affects sediment generation rates derived from $^{10}Be_i$. If disturbance is shallower than the mixed layer, $^{10}Be_i$-determined sediment generation rates are not altered by the disturbance. If the weathering front is shallow, $^{10}Be_i$-derived sediment generation rates largely include the effects of chemical weathering. However, $^{10}Be_i$-determined sediment generation rates will underestimate the total mass flux from the landscape as the weathering front deepens. Inset shows different integration times for $^{10}Be_i$, sediment yield, and land use. (B) Distribution of river mass load between bed, suspended, and dissolved loads is different for every river. The proportions shown are representative of the study region (Summerfield and Hulton, 1994). The ratio of sediment yield to $^{10}Be_i$-derived sediment generation rate will be underestimated if only suspended load, and not bedload, is considered.

speaking, rainfall increases from north to south in the study area. The large catchments along the main stem Yangtze, Salween, and Mekong Rivers are the driest while the smaller catchments on tributaries to the Mekong in the southern parts of the study area are the wettest.

None of the watersheds sampled have significant percentages of glacial cover at the present time, and thus are unlikely to have been significantly affected by Holocene glaciation. Holocene climate in the region has been relatively stable, as evidenced by no major glacial

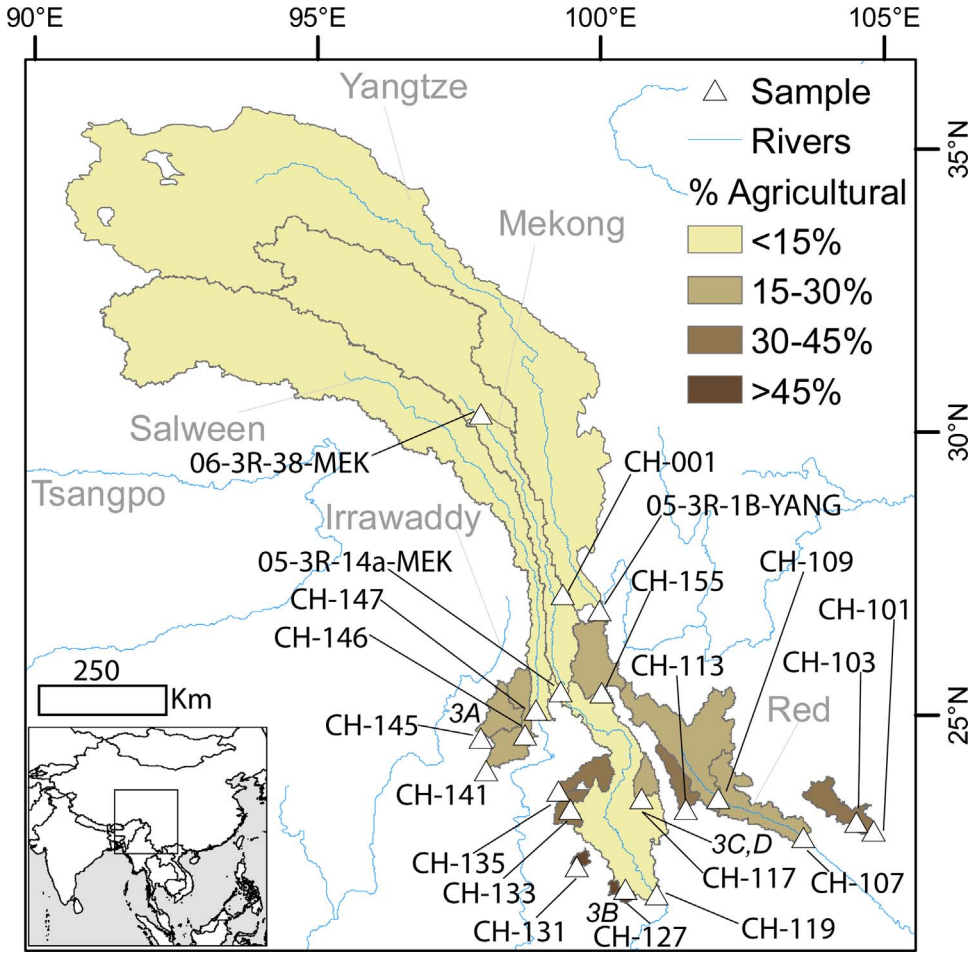

Fig. 2. Context map showing major rivers, gauging station and sediment sample locations, watershed boundaries, and land use for the upstream watersheds. Often several stations are located on the same river. Watershed areas shown, and thus upstream land use, only depict the unique area sampled by each station. Inset map shows study area in the context of Asia. Labels in italics (3A, 3B, 3C,D) identify the watersheds where photos in Fig. 3 were taken.

Fig. 3. Watershed field photos (locations labeled in Fig. 2). (A) Reforestation projects have established monocultures along steep slopes. (B) Rice paddies are common. (C) Agricultural practices include slash and burn. (D) In river sand/gravel mining is ubiquitous.

advances (Schäfer et al., 2002). Work in the eastern Tibetan Plateau (Litang area, just north of our study region) suggests that even during the last glacial maximum (24–13 ka), glaciers did not extend more than ~10 km further down valley than they do at present (Schäfer et al., 2002). Erosion rates are high enough that any glaciation during the Pleistocene has little effect on $^{10}Be_i$ concentrations measured today.

Current land use in our sampled catchments ranges from 0 to 54% agricultural (Fig. 2), with agricultural use generally increasing from north to south (Chen et al., 2015). Thus, the main stem Salween, Yangtze, and Mekong samples, which represent the largest upstream areas, have minimal (< 5%) agricultural area; in contrast, the watersheds on the rainier, flatter slopes in the southern parts of the study area are the most agricultural. Field observations suggest that agricultural land use includes cultivation of rice, sugar cane, bananas, tea, and rubber trees. We observed monocultures on steep slopes, sometimes all the way to the river, and slash-and-burn agricultural practices (Fig. 3). In addition, furrows on agricultural fields are frequently parallel to the hillslope rather than perpendicular; we assume this furrowing is to facilitate drainage during the wet growing season.

Human impacts in river channels (dams, gravel mining, irrigation diversions, channel straightening) are common in the study area (Fig. 3). We mapped dam locations (using Google Earth) upstream of each sample site and find that 7 of 20 sample sites have no dams that are visible on Google Earth within 100 km upstream. The remaining 13 sample sites are downstream of dams. The 13 sites are 0.2–43 km (median = 12 km) downstream of dams. Dams in the region post-date the sediment yield data (Magee, 2006), all of which were collected prior to 1987. In stream gravel mining is ubiquitous in the region. We tried to sample upstream of gravel mines where possible, but likely were downstream of other gravel mining operations. In addition, in some watersheds, major channel alterations such as straightening and water diversion for irrigation were common. In one extreme case (CH-127), the main channel was not identifiable in parts of the watershed due to human modification.

China has had a centralized, active land management program for many years. Following catastrophic flooding on the middle Yangtze River in 1998, the Chinese government implemented the Natural Forest Protection Program and the Returning Farmland to Forest Program, among the world's largest payment for ecosystem services programs (Chen et al., 2009). The programs' goals were to decrease erosion in headwater regions through controversial bans on deforestation and agriculture on steep slopes and mandatory reforestation of these lands (Brandt et al., 2012; Trac et al., 2007, 2013; Zhang et al., 2014). The 1998 Yangtze River floods are blamed by the government on deforestation and increased agriculture during the Three Great Cuttings (the Great Leap Forward [late 1950s], Grain as the Key Link [early 1970s], and Opening and Development [mid-1980s]) (Shapiro, 2001; Trac et al., 2007). However, prior large scale research has been inconclusive on the role of human activity in increasing sediment yield rates (Lu et al., 2003a, 2003b; Schmidt et al., 2011). In contrast, small scale studies of land use and erosion from the 1950s to present suggest that deforestation and increases in agriculture have greatly increased erosion in western China (Shapiro, 2001; Urgenson et al., 2010). There are three possible ways to reconcile these data: erosion increased locally but increases were not widespread enough to increase sediment yield in large rivers, eroded material is stored in floodplains and alluvial fans and has not exited the watershed in rivers, or sediment yield was elevated during the entire sediment gauging period of record (1950s–1980s) (Schmidt et al., 2011).

4. Methods

4.1. Field methods

We collected medium sand-size (250–850 μm) sediment samples from active river channels and floodplains to analyze for both *in situ* and meteoric ^{10}Be ($^{10}Be_i$ and $^{10}Be_m$, respectively) at 20 sites at or near Chinese-operated gauging stations for which there are discharge and

suspended sediment data available for 4 to 26 years between 1945 and 1987 (Schmidt et al., 2011). Samples were collected from alluvial rivers in landscapes with varying degrees of agricultural land use. Agriculture on river banks and dredging of river channels for gravel were common; when possible, we collected samples upstream of dredging operations. Three samples (05-3R-1b-YANG, 05-3R-14a-MEK, and 06-3R-38-MEK) were collected in 2005 and 2006; all others were collected in 2013 and 2014. For most sample sites (all except CH-146, 05-3R-1b-YANG, 05-3R-14a-MEK, 06-3R-38-MEK), we collected between 2 and 4 samples at each site (in channel and overbank, samples collected 1–3 km apart, and/or in both 2013 and 2014). The $^{10}Be_i$ and $^{10}Be_m$ concentrations we report for each station represent an uncertainty-weighted average and standard deviation of these spatial and temporal replicate samples to reduce uncertainty due to variability in sediment moving through the rivers (Gonzalez et al., 2017).

4.2. Basin average parameters

We used the 30 m GDEM topographic dataset (NASA LP-DAAC, 2012) to determine watershed boundaries as well as effective elevation, slope, and upstream area for each watershed. Rainfall data are taken from the APHRODITE dataset (Yatagai et al., 2012). This dataset is coarser than other available datasets for rainfall in the region, but has better spatial and temporal accuracy (Andermann et al., 2011).

Land use was determined from the Global Land Cover (GLC) dataset (Chen et al., 2015). For each basin, we determined the percent of the upstream area that is agricultural from the “cropland” classification. However, this underestimates cropland for our watersheds because orchards are classified as forested. In the field, we observed numerous banana and rubber plantations in the study area, but these locations are classified as “forest” in the GLC dataset. Likewise, tea plantations we observed in the field are classified as shrubs. Thus, percent agricultural land is a minimum value, particularly in southern parts of the region, where banana and rubber plantations are most common. In addition, because the land use data are based on images taken between 2000 and 2010, and the suspended sediment data are for 1945–1987, there is a mismatch in time that may induce other errors into the analysis. Given expansion of agriculture in China during the 1950s-1970s as well as recent development, it is likely that any errors in the land use data are not systematic over or underestimates of agricultural land relative to the time of the gauging station data.

4.3. ^{10}Be data

Quartz from the samples was isolated and purified through a series of acid etches using a modification of the method of Kohl and Nishiizumi (1992). $^{10}Be_i$ was extracted from quartz following the method of Corbett et al. (2016). Each batch contained one process blank and one CRONUS N standard (Jull et al., 2015). Once the quartz was dissolved in hydrofluoric acid, aliquots were removed and analyzed by inductively coupled plasma-optical emission spectroscopy (ICP-OES) to measure Be and Al content (Corbett et al., 2016; Portenga et al., 2015). 10 samples had Be recovery $>100\%$ (range: 102.6–198.1%) (based on the Be carrier added), indicating the presence of native Be in those samples. For $^{10}Be_m$ analysis, samples were first milled, and a small ($\sim$0.5 g) aliquot of pulverized material was used for isotopic extraction. We used the method of Stone (1998) to extract $^{10}Be_m$ with the addition of cation exchange to reduce B interference.

Isotopic ratios were measured using Accelerator Mass Spectrometry (AMS) at the Scottish Universities Environmental Research Centre in East Kilbride, Scotland (Xu et al., 2015) and normalized to the NIST standard with an assumed $^{10}Be/^{9}Be$ ratio of 2.79×10^{-11} (Nishiizumi et al., 2007) (Table DR1). Background correction was done using full process blanks, one of which was run with each batch of 10 *in situ* samples and 14 meteoric samples. For quartz with native ^{9}Be, we used the total Be from ICP measurements to calculate ^{10}Be concentration (Portenga et al., 2015). The final uncertainty of the blank-corrected ratio is the uncertainty of the isotopic measurement and the blank propagated in quadrature.

Background sediment generation rates [tons $km^{-2}\,yr^{-1}$] were calculated from $^{10}Be_i$ concentrations using the CRONUS Earth Calculator Version 2.3 (http://hess.ess.washington.edu/) (Balco et al., 2008). To make this estimate, we calculated the effective elevation of each watershed using the approach of Portenga and Bierman (2011) (Table DR2). We did not adjust calculations for watersheds with dams, but recognize that this could result in overestimating sediment generation rates for samples taken in close proximity to dams if those dams effectively restrict or cut off sediment supply from upstream − something unknowable without extensive fieldwork and details of the dam operations (Reusser et al., 2017). We used the time-invariant scaling scheme of Lal (1991) and Stone (2000) and the global production rate of $^{10}Be_i$ (Borchers et al., 2016). To calculate background sediment generation rates, we assume a long-term sediment delivery ratio of one (i.e., all sediment eroded is exported in the rivers and there is no net storage in the watershed), and that no eroded material is lost in solution. This means that our background sediment generation rates likely underestimate actual mass lost because some mass is lost by dissolution.

The assumption of no significant net sediment storage is reasonable over long time scales. In our study area, the mountainous topography and relatively high $^{10}Be_i$ erosion rates suggest that the percentage of sediment stored during transport is minimal over geologic time scales (i.e., how long it takes to erode one attenuation length, $\sim$60 cm of rock). Field observations confirm that although some catchments retain some alluvium, including terraces (seen in 5 out of 20 catchments), it is unlikely that total alluvial volume is more than a small percentage of the total sediment flux out of these steep, predominately mountainous catchments.

4.4. Contemporary sediment yield data

We use the contemporary sediment yield for 20 rivers (Schmidt et al., 2011), based on discharge and suspended sediment data from the Chinese Ministry of Hydrology (http://www.oberlin.edu/faculty/aschmidt/chdp/index.html). Dissolved and bedload data are not available. The Mekong River is reported as having $\sim$13% of the total river mass load as dissolved load and globally bedload is $\sim$10% of the suspended load (Summerfield and Hulton, 1994). We only consider the suspended solid river load in this paper. Thus, because we only have suspended sediment data, reported contemporary sediment yields are an underestimate of actual contemporary rates of sediment leaving basins. We recalculated sediment yields from the original daily data because in some cases upstream basins and areas were based on better knowledge of the station location either from the field (i.e., we found the actual station) or from online resources available from the Chinese Ministry of Hydrology. Annual sediment yields are not normally distributed for any station (Figure DR2). Thus, instead of reporting mean annual sediment yield, we use median annual sediment yield and report the interquartile range as the uncertainty to minimize the effects of outlier data. This results in a conservative estimate of contemporary sediment yield that may underrepresent the contemporary average because of the importance of rare but massive events that may be captured in a single year of data. We divided the contemporary sediment yield by the background sediment generation rate to obtain a ratio, and discuss our findings in terms of this ratio. We do not have the original data for the Shigu station and so we use mean and standard deviation for all calculations, as reported by Higgitt and Lu (1996). Because our data are only suspended sediment data and do not include bedload, we are underestimating contemporary sediment yield and thus also underestimating the ratio of contemporary sediment yield to long-term sediment generation.

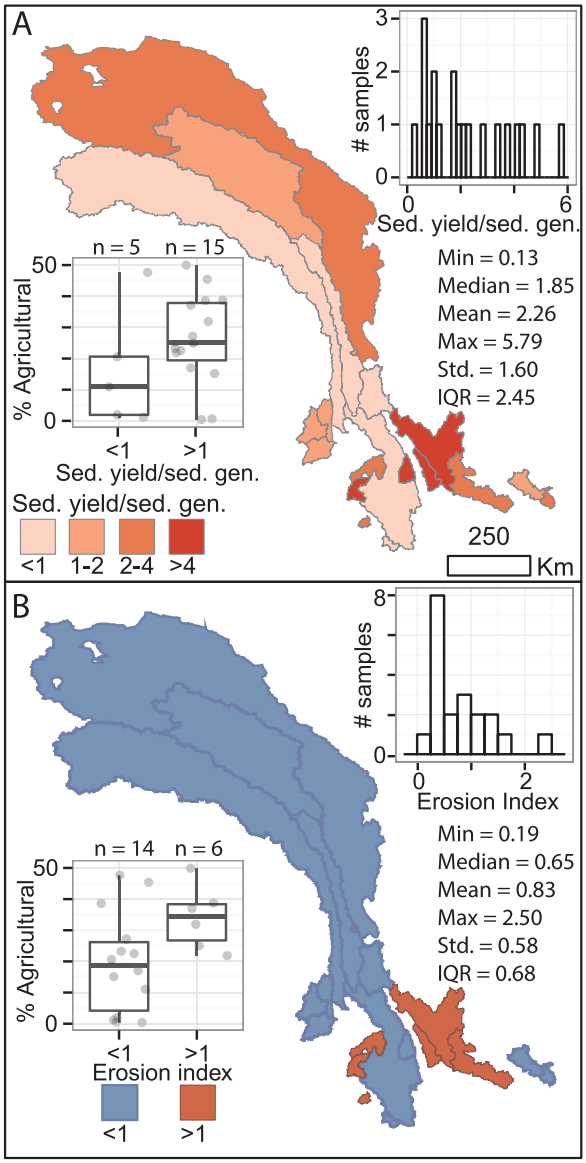

Fig. 4. Summary of results. Spatial variations in (A) sediment yield/sediment generation ratios and (B) erosion indices are shown across the study area. Upper right insets show the structure of the data depicted on each map. Lower left insets show agricultural land as a function of sediment yield/sediment generation ratios and erosion indices grouped to above and below one. For boxplots, the median is the middle line, the 25th and 75th percentiles are the edges, and whiskers extend to include all samples within 1.5 times the range of the box; outliers fall outside this range. Grey points are data summarized by boxplots. Under the histograms are summary statistics for the data in the figure. Std. is the standard deviation; IQR is the interquartile range. See table DR3 for data.

4.5. Erosion indices

We calculate erosion indices (*EI*) (Brown et al., 1988) using the equation,

$$EI = M\eta'/Aq, \quad (1)$$

where M is the annual sediment load (g/yr), η' is the $^{10}Be_m$ concentration (atoms/g) in sand-sized material leaving the basin, A is the basin area (cm^2), and q is the atmospheric deposition rate of $^{10}Be_m$ in the watershed (atoms cm^{-2} yr^{-1}). The value of q for each watershed was calculated as per Graly et al. (2011), and contributes 20% uncertainty to the calculations, as they report 20% confidence in delivery rates at low latitudes. We calculated M using median measured contemporary suspended sediment load; uncertainty in sediment yield is the interquartile range in the sediment load. Uncertainties from $^{10}Be_m$ deposition and sediment load are propagated in quadrature. We only have suspended sediment data for M, thus we are underestimating the erosion indices because bedload is not included.

4.6. Statistical methods

Due to the non-normal distribution of all datasets (annual sediment yield at each individual station, median contemporary annual sediment yield among stations, long term sediment yield among stations, and all upstream basin parameters – area, rainfall, slope, and land use), we use only non-parametric statistics for our analyses. We use the Wilcoxon signed-rank test (a paired test) to determine if long term sediment generation is different from contemporary sediment yield; this test distinguishes noise from statistically significant differences between populations of data. We use the Mann Whitney U test to determine if mapped agricultural land use among watersheds with the sediment yield/sediment generation ratio and erosion index > 1 is different from the land use among watersheds with the sediment yield/sediment generation ratio and erosion index < 1. We use Spearman Rank Correlation to determine correlation coefficients (rho) for regression analyses. Rho ranges from -1 to 1, with 0 being no correlation (the null hypothesis), -1 being a perfect inverse correlation, and 1 being a perfect direct correlation. For more details on statistical methods, including tests of normality, see the Supporting information.

5. Results

5.1. Ratios of contemporary sediment yield to background sediment generation rates

We find that, on average, sediment is being transported out of the watersheds we studied approximately twice as rapidly as it is being generated (sediment yield/generation ratios from 0.13 to 5.79, mean = 2.18, median = 1.85). Long term sediment generation rates for our watersheds, calculated from $^{10}Be_i$ and assuming that all eroded material is exported as sediment, range from 43.3 to 804 tons km^{-2} yr^{-1} (median = 288; interquartile range = 195; Table DR3). Contemporary sediment yields calculated from hydrology station data range from 77.2 to 1720 tons $km^{-2}yr^{-1}$ (median = 455, interquartile range = 504; see figure DR2 for box plots showing the distribution of all annual data for each station) (Schmidt et al., 2011). There is a statistically significant difference between the contemporary sediment yields and long term sediment generation rates when considering the population of all stations ($n = 20$, $p < 0.05$). Ratios of contemporary sediment yields and long term sediment generation rates range from 0.13 to 5.79 (median = 1.85, interquartile range = 2.45). For 14 out of 20 sites that we compared, the contemporary sediment yield is higher than the sediment generation rate (Fig. 3B). Of the six remaining sites with higher long term sediment generation rates (ratios range from 0.13 to 0.92), three drain the high, flat Tibetan Plateau and the sparsely populated and rapidly eroding gorges of the Three Rivers Region (specifically, the Salween and Mekong Rivers) and three are samples taken within 2 km downstream of dams (as expected from the analysis of Reusser et al., 2017).

We find that the watersheds with contemporary sediment yields higher than long-term rates of sediment generation have, on average, a median of 25% agricultural land (interquartile range = 19%; $n = 14$), compared to a median agricultural land use of 11% in watersheds where the contemporary sediment yield is lower than the long term sediment generation rate (interquartile range = 19%; $n = 6$). Furthermore, we find that upstream agricultural land use is directly and significantly correlated with the sediment yield/sediment generation ratio (Spearman rank correlation rho = 0.52, $p < 0.05$, Fig. 5). Neither rainfall nor agricultural land use are correlated with contemporary sediment yield ($|rho| \leq 0.28$, $p > 0.05$, Fig. 5) and contemporary sediment yield and long term sediment generation rate are not correlated with each other (rho = 0.32, $p = 0.36$).

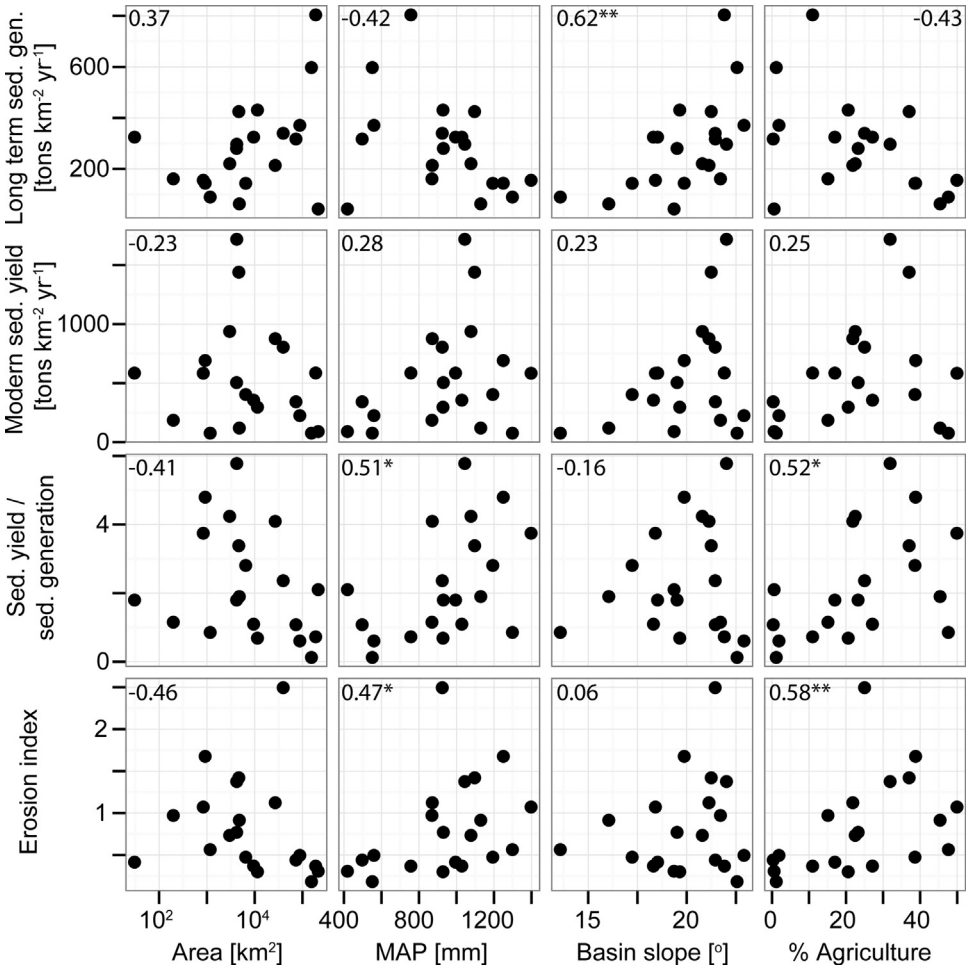

Fig. 5. Derived erosion parameters as a function of average upstream basin parameters. From top to bottom, erosion parameters are: $^{10}Be_i$-derived long term sediment generation rates, contemporary sediment yield (median of annual sediment yields for each station), sediment yield/sediment generation ratio, and erosion index (from sediment yield and $^{10}Be_m$ concentrations). From left to right, upstream parameters are: area, mean annual precipitation (MAP), mean basin slope, and fraction of the upstream area mapped as agricultural land use. The Spearman correlation coefficient (rho) is shown for each plot. * indicates significance at $p < 0.05$, ** indicates $p < 0.01$.

5.2. Meteoric ^{10}Be erosion indices

Taken at face value, erosion indices (EI; Fig. 4C) suggest that less $^{10}Be_m$ is exported from than delivered to many of the watersheds we sampled (EIs ranges from 0.18 to 2.50; median = 0.65, interquartile range = 0.68); 14 of the 20 sites have EI < 1 indicating net storage. However, this metric is flawed; the erosion indices we calculate are minima because we analyzed the medium sand fraction of riverine sediment (for direct comparison with $^{10}Be_i$ data) and $^{10}Be_m$ has an affinity for fine grain material (Singleton et al., 2017; Wittmann et al., 2012) (see Supporting information). There is no reliable means to correct for the grain-size bias because we do not know and could not measure the grain-size specific sediment yield over time for each river we sampled; thus, sampling fine grain material would not address this issue. In addition, by only using suspended sediment in the EI calculation (*M* in the numerator), we are further underestimating EI because bedload is not considered.

We can work around this limitation by considering the relationship between measured EI and the fraction of upstream land under cultivation. We find a direct and significant correlation between percent agricultural use and erosion index in our sampled watersheds (Spearman correlation coefficient rho = 0.58, $p < 0.01$, Fig. 5). Furthermore, agricultural land use in basins exporting more $^{10}Be_m$ than is being delivered (EI > 1: median = 34% agricultural land, interquartile range = 12%, n = 6) is greater than in basins exporting less $^{10}Be_m$ than is being delivered (EI < 1: median = 19% agricultural land, interquartile range = 32%, n = 14) ($p = 0.05$ for a Mann-Whitney *U* test).

6. Discussion

Our new data from China suggest that contemporary sediment yield is elevated by a median factor of two compared to background sediment generation rates (ratios from 0.13 to 5.79, mean = 2.18, median = 1.85). Below, we explore the processes that could be causing the increase in contemporary sediment yield. We then put our data into context with a global compilation of studies that compare contemporary sediment yield to background sediment generation rates. Finally, we consider the additional information that can be gained from the $^{10}Be_m$-derived erosion indices.

6.1. Ratios of contemporary sediment yield to background sediment generation

The sediment generation and sediment yield data are consistent with deforestation and agricultural land use increasing contemporary sediment yields over background rates of sediment generation. Fourteen of the twenty watersheds analyzed have sediment yield/sediment generation ratios > 1 (median = 1.85). Our field observations of monocultures on steep slopes, in many cases reaching the river banks, agriculture in floodplains, and “slash and burn” practices support the observation that land use increases contemporary sediment yield by rapidly, frequently, and directly supplying sediment to river channels (Fig. 3).

Six of the twenty watersheds have sediment yield/sediment generation ratios < 1. Three of these watersheds (CH-127, CH-146, and CH-155) are the only watersheds with samples taken less than 2 km downstream of dams. Proximity to dams is likely affecting the supply of sediment and altering the $^{10}Be_i$-derived erosion rates by disconnecting

the sample site from the upstream environment, especially because any available terrace sediment is unlikely to be reworked over such a short distance (Reusser et al., 2017). In addition, one of these watersheds (CH-127) contains primarily agricultural land used for rice cultivation in paddies. In this case, the entire watershed is filled with dams that are impeding the movement of sediment out of the system. Because sediment yield data predate 1987 and most dams in the region post-date 1987 (Magee, 2006), we have not corrected the $^{10}Be_i$ production rate calculations for the samples taken in close proximity to dams. If we were to do that, we would be comparing erosion rates for the area only downstream of the dam to sediment yield data for the entire watershed. Instead, we recognize that sediment generation rates for watersheds where samples are taken in close proximity to dams are likely too high (Reusser et al., 2017), and thus sediment yield/sediment generation ratios for these watersheds are too low.

The other three samples with sediment yield/sediment generation ratios < 1 (0.13–0.73) are unlike other samples in our data set because they were taken on the main stem Salween and Mekong Rivers (CH-119, CH-147, 05-3R-14a-MEK; area $> 85{,}000\ km^2$, agricultural land use $\leq 1\%$). Several factors unique to these samples may account for their low sediment yield/sediment generation ratios. Overall, there is little agriculture in the main stem Salween and Mekong basins ($\leq 1\%$). However, two large Yangtze and Mekong watersheds (area $> 77{,}000\ km^2$) have low agricultural land use ($\leq 2\%$) and sediment yield/sediment generation ratio > 1 (2.10 and 1.08, respectively). Thus, it seems unlikely that low agricultural land use is the only explanation for the low sediment yield/sediment generation ratios for the main stem Salween and Mekong samples. Sediment storage in these large river systems may buffer against increased sediment yield resulting from land use change (Schmidt et al., 2011). However, large basins on the Yangtze and Red Rivers (area $> 26{,}000\ km^2$) have sediment yield/sediment generation ratios > 2 (2.10–4.10).

We conclude that the most likely explanation for the low sediment yield/sediment generation ratios at the main stem Mekong and Salween locations is the high erosion rate through the Three Rivers Region gorge. The rapidly eroding gorges in the Three Rivers Region (Henck et al., 2011) add enough sediment that they swamp any upstream land-use signal in samples taken from that area because stochastic events not captured in short-term sediment yield records bias contemporary sediment yields downward (Kirchner et al., 2001). The large watersheds on the Mekong, Red, and Yangtze Rivers with higher sediment yield/sediment generation ratios (1.08-4.10) have lower background erosion rates (≤ 0.12 mm/yr) than the three watersheds draining the Mekong and Salween gorges of the Three Rivers Region (0.14–0.30 mm/yr).

6.2. Influence of human activity on sediment yield/sediment generation ratios

The influence of topography, climate, and land use on sediment yield/sediment generation ratios is complicated – because these boundary conditions likely affect both long term sediment generation and contemporary sediment yield estimates, but perhaps in different ways. We find that none of the parameters we considered (slope, rainfall, agricultural land use, basin area, or sediment generation rates) are correlated with contemporary sediment yield ($|rho| \leq 0.32$, $p > 0.05$, Fig. 5). This could be because precipitation, agricultural land use, and basin slope are often found to be drivers of high sediment yields (e.g., Higgitt and Lu, 1996; Reusser et al., 2015; Schmidt et al., 2011), but because slope is inversely proportional to precipitation and agricultural land use in this region, the parameters effectively cancel each other out.

As with studies of background erosion rates in eastern Tibet (Henck et al., 2011; Hetzel, 2013; Kirby and Harkins, 2013; Ouimet et al., 2009), we find that long term sediment generation is best, and directly, correlated with mean basin slope (rho = 0.62, $p < 0.01$; Fig. 5). Although neither contemporary sediment yield nor long term sediment generation are correlated with rainfall or agricultural land use, the sediment yield/sediment generation ratio is positively correlated with both ($rho \geq 0.51$, $p < 0.05$); rainfall and agricultural land use are significantly, strongly, and directly proportional to each other (rho = 0.95, $p < 0.01$; Figure DR3). Thus, it could be that rainfall is driving patterns in both land use (because people prefer to farm in places with more rain) and sediment yield/sediment generation ratio. However, if rainfall were the driving factor, we would expect to see a signal of rainfall in the long term sediment generation, as prior studies in other regions have (Dixon et al., 2009; Reiners et al., 2003), but we do not. Therefore, agricultural land use is likely the primary driver of the trends in sediment yield/sediment generation ratio we observe. More specifically, we conclude that the correlation we observe between sediment yield/sediment generation ratio and agriculture is driven by increases in contemporary sediment yield relative to background rates of sediment generation in watersheds with low slope, high rainfall, and thus high rates of agriculture.

6.3. Comparison to global data

Studies comparing contemporary sediment yield to millennial-timescale measures of sediment generation, including this study, vary considerably in their findings (Fig. 6; Table 1). Landscape sediment yield/sediment generation ratios approaching one are typically considered to be in mass steady state (Willett and Brandon, 2002). Studies of the Amazon Basin, the Yangtze Basin, and the Great Smoky Mountains, although there is a lot of scatter in the data, find ratios that are close to one (Chappell et al., 2006; Matmon et al., 2003; Wittmann and von Blanckenburg, 2009; Wittmann et al., 2011).

Deviations from steady state in which ratios are > 1 are common in areas where human agricultural land use has altered the landscape (Bartley et al., 2015; Hewawasam et al., 2003; Regard et al., 2016; Reusser et al., 2015; Vanacker et al., 2014; Vanmaercke et al., 2015). Hewawasam et al. (2003) report a median sediment yield/sediment generation ratio of 6.24 for watersheds ranging from 16 to 731 km^2. Their maximum ratios are > 30 and from watersheds up to 731 km^2. Reusser et al. (2015) find that hundreds of years of intensive agriculture in the eastern US elevated contemporary sediment yield by a median factor of 2.78 relative to millennial rates of sediment generation for watersheds up to 16,376 km^2. In the same area, they report even higher hillslope erosion rates (based on the work of Trimble (1977) and Costa (1975)) and that most of the eroded hillslope sediment is stored as colluvium in toe slopes (Reusser et al., 2015). A study in Europe compared contemporary sediment yield measurements in agricultural basins to the modeled sediment yield of those same basins if they were undisturbed, forested landscapes (Vanmaercke et al., 2015). Vanmaercke et al. (2015) find a strong human influence on sediment yield in small watersheds ($< 100\ km^2$), but not in watersheds $> \sim 10^3\ km^2$.

For the new China data, we find sediment yield/sediment generation ratios up to 5.79 for watersheds as large as 213,260 km^2. However, the bulk of our watersheds with ratios > 1 (12 of 14) are for watersheds smaller than 40,000 km^2. We find a statistically significant difference in basin area for basins with sediment yield/sediment generation ratios > 1 compared to < 1 ($p < 0.05$, Mann-Whitney U test). Thus, it seems that in a variety of climates and locations, agricultural land use can increase sediment yield in the short term, even for large watersheds, although large watersheds are more likely to buffer against fluctuations in sediment yield (Vanmaercke et al., 2015).

Deviations from steady state where sediment yield/sediment generation ratios are < 1 frequently happen in small watersheds. These studies interpret the low ratios as evidence that infrequent, large mass wasting events are driving long term rates of erosion and sediment transport (Covault et al., 2011; Ferrier et al., 2005; Kirchner et al., 2001; Meyer et al., 2010a, 2010b; Regard et al., 2016; Schaller et al., 2001; Siame et al., 2011; Warrick and Farnsworth, 2009). We find some

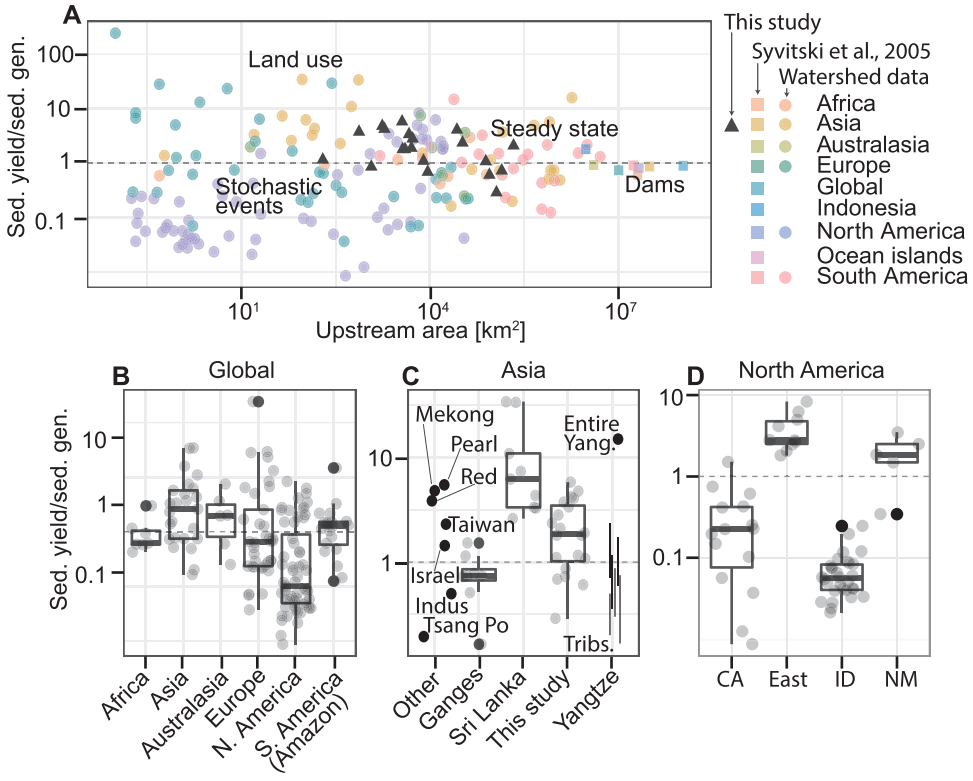

Fig. 6. Sediment yield/sediment generation ratios vary considerably depending on both basin area and study location. Dashed line represents a ratio of one, i.e., contemporary sediment yield equals background timescale sediment generation. (A) Prior analysis finds ratios ranging from 0.009 to 34.4 (mean = 2.0, median = 0.60). For the largest areas, ratios < 1 are attributed to dams trapping sediment. For smaller basins, ratios < 1 are attributed to high-magnitude, low-frequency events that increase background rates but are not captured in shorter sediment yield records (stochastic events). Ratios ~1 are attributed to landscape steady state. Ratios > 1 are attributed to land use. (B) Box plots showing watershed measurements by continent (as reported in Bartley et al., 2015; Bierman et al., 2005; Clapp et al., 2002; Clift, 2006; Covault et al., 2013, 2011; Ferrier et al., 2005; Hewawasam et al., 2003; Kirchner et al., 2001; Lupker et al., 2012; Meyer et al., 2010a, 2010b; Milliman and Meade, 1983; Regard et al., 2016; Reusser et al., 2015; Schaller et al., 2001; Schmidt et al., 2011; Siame et al., 2011; Vanacker et al., 2014; Warrick and Farnsworth, 2009; Wittmann et al., 2009, 2011). (C) Boxplots and data points for Asian analyses organized by location. (D) Boxplots for North American analyses organized by location.

Table 1
Summary of prior studies comparing short-term sediment yield to longer-term sediment generation. We have turned all data into sediment yield/sediment generation ratios as defined in our methods section. Many, but not all, of these studies were previously compiled in Covault et al. (2013). Individual data points summarized in this table are in table DR4.

Study	Location	Number of samples	Median watershed area (km^2) (range in parentheses for studies with more than one sample)	Median sediment yield to sediment generation ratio (range in parentheses for studies with more than one sample)
Bartley et al. (2015)[a]	Australia	6	13,365 (14–36,140)	1.97 (0.25–7.47)
Bierman et al. (2005)	New Mexico	5	7122 (1117–16,153)	1.85 (0.34–2.50)
Chappell et al. (2006)	Yangtze River basin, China	Not reported	Not reported	Only ranges reported (0.17–2.33)
Clapp et al. (2002)	Israel	1	0.6	1.38
Clift (2006); Milliman and Meade (1983)[b]	Yangtze, Indus, Pearl, Mekong, Red Rivers at their outlets	5	795,000 (143,700–1,808,500)	4.93 (0.49–15.93)
Covault et al. (2011); Warrick and Farnsworth (2009)[c]	California	5	894 (339–1851)	0.10 (0.0086–0.61)
Ferrier et al. (2005)	California	10	4.62 (0.21–720.45)	0.25 (0.037–1.51)
Hewawasam et al. (2003)	Sri Lanka	9	106.77 (16–731.33)	6.24 (2.61–34.35)
Kirchner et al. (2001)	Idaho	30	1.55 (0.22–34,773.1)	0.06 (0.021–0.25)
Meyer et al. (2010a)	Germany	2	120.2 (64.7–175.7)	0.69 (0.69 − 1.68)
Meyer et al. (2010b)[a]	Germany	6	170.95 (88.9–396.8)	0.29 (0.19–0.66)
Lupker et al. (2012)	Ganges River	8	109,850 (7600 − 935,000)	0.74 (0.16 − 1.53)
Reusser et al. (2015)	Eastern US	10	7612.5 (2987–16,376)	2.78 (1.81–8.33)
Schaller et al. (2001)	Western Europe	11	12,676 (432–40,600)	0.23 (0.04–0.84)
Schmidt et al. (2011)[d]	Tsang Po River, Tibet	1	203,904	0.20
Siame et al. (2011)	Taiwan	1	376.4	2.3
Syvitski et al. (2005)[e]	Global	25	1.70×10^7 (10^5–10^8)	0.89 (0.30–3.33)
Vanacker et al. (2014)[a]	Europe	18	1.31 (0.1–276)	3.79 (0.07–243)
Wittmann and von Blanckenburg (2009)	Amazon basin	12	96,000 (1600–954,000)	1.20 (0.23–14.81)
Wittmann et al. (2011)	Amazon basin	8	782,500 (213,000–5,088,000)	1.38 (0.12–2.17)

[a] They report contemporary sediment yield as the sum of suspended, dissolved, and bedload, so reported contemporary loads are higher than for most studies, which just consider suspended loads.

[b] We compiled this comparison from data published in these two papers. The data compare suspended sediment to delta deposition rates.

[c] These data are compiled in Covault et al. (2013) but not either of the original papers.

[d] Schmidt et al. (2011) report data for five watersheds based on four sample/gauging station pairs. One of the watersheds they report is for the nested area between two sample/gauging station pairs. We only report one data point here from that paper because we are using the other three samples from their study in this paper with new $^{10}Be_m$ data.

[e] This is a global modelling study.

of the largest examples of these effects on landscapes in our main stem Salween and Mekong watersheds, which are among the steepest watersheds we sampled (mean basin slope ≥22°).

Deviations from steady state where sediment yield/sediment generations ratios are < 1 in larger watersheds are interpreted as evidence of sediment storage over decades (Covault et al., 2013; Schmidt et al., 2011; Syvitski et al., 2005). Syvitski et al. (2005) compiled sediment yield/sediment generation ratios at the continental scale and argue that dams along rivers are artificially depressing contemporary sediment yields and thus lowering the sediment yield/sediment generation ratio (Fig. 6). We see the effects of dams on $^{10}Be_i$-derived sediment yields in three of our sites with low ratios, primarily due to overestimating sediment generation for samples collected in close proximity to dams (Reusser et al., 2017).

6.4. Meteoric ^{10}Be-derived erosion indices

The positive correlation between EI and agricultural land use is consistent with agriculture increasing the export of sediment and $^{10}Be_m$. This correlation is driven by the modest positive correlation between $^{10}Be_m$ and agricultural land use (rho = 0.41, p = 0.08); EI is also controlled by contemporary sediment yield, but there are no statistically significant correlations for contemporary sediment yield and any of the upstream basin factors considered (Fig. 5). The analysis of different agricultural land use for erosion indices greater and less than one again suggest that agriculture mobilizes sediment and the associated $^{10}Be_m$, and then delivers that sediment to rivers. Our findings echo those of Brown et al. in eastern North America, who found that erosion indices increased in areas with intensive agriculture (Brown et al., 1988). Erosion indices also provide evidence of the sediment buffering effects of small dams (Walter and Merritts, 2008); for example, some watersheds with low erosion indices and high agricultural land use have widespread rice paddies. These rice paddies act as small dams and reduce the out-flux of $^{10}Be_m$ through temporary sediment storage (e.g., CH-127, shown in Fig. 3B).

7. Conclusions

Here, using data from 20 rivers draining a variety of Chinese landscapes, we show that land use change (human impact) increased contemporary sediment yield to a median of twice the background rate sediment generation. Using erosion indices, we show that $^{10}Be_m$ is preferentially lost from most of the watersheds studied, particularly those with higher rates of agricultural land use. Agricultural land use is directly proportional to the ratio of contemporary sediment export to sediment generation and to erosion indices, suggesting a strong agricultural influence on the loss of sediment from these watersheds. Such erosion in response to land-use change is likely to have adversely affected ecosystem services in the study area by increasing river sediment load in rivers, altering benthic environments and potentially burying spawning grounds (Gellis et al., 2017), increasing siltation behind dams (Wang et al., 2005), and increasing sediment associated nutrients in river sediment (Walling et al., 2003).

Acknowledgements

Supported by funding from the US National Science Foundation awarded to A. H. Schmidt (NSF-EAR-1114166), P. Bierman (NSF-EAR-1114159), and D. H. Rood (NSF-EAR-1114436). Field work was also supported by a State Key Laboratory Open Fund (China) Grant to A. H. Schmidt. We thank D. McPhillips for collecting and providing sample Y13-01-DM, J. Martin for GIS assistance, the staff of the AMS laboratory at SUERC for support during isotopic analyses, I. Larsen, D. Montgomery, G. Govers, G. Balco, and five anonymous reviewers for feedback on early versions of the manuscript, H. Glasman-Deal for editorial comments, and C.M. Zhang, R.J. Wei, J.A. Bower, A. Singleton, and Y. Qiu for field assistance.

Appendix A. Supplementary data

Supplementary data associated with this article can be found, in the online version, at https://doi.org/10.1016/j.ancene.2017.10.002.

References

Akciz, S., Burchfiel, B.C., Crowley, J.L., Yin, J.Y., Chen, L.Z., 2008. Geometry, kinematics, and regional significance of the Chong Shan shear zone, Eastern Himlayan Syntaxis, Yunnan, China. Geosphere 4 (1), 292–314. http://dx.doi.org/10.1130/GES00111.1.

Amundson, R., Berhe, A.A., Hopmans, J.W., Olson, C., Sztein, A.E., Sparks, D.L., 2015. Soil and human security in the 21st century. Science 348 (6235).

Andermann, C., Bonnet, S., Gloaguen, R., 2011. Evaluation of precipitation data sets along the Himalayan front. Geochem. Geophys. Geosy. 12 (7), Q07023.

Balco, G., Stone, J.O., Lifton, N.A., Dunai, T.J., 2008. A complete and easily accessible means of calculating surface exposure ages or erosion rates from ^{10}Be and ^{26}Al measurements. Quat. Geochronol. 3, 174–195.

Bartley, R., Croke, J., Bainbridge, Z.T., Austin, J.M., Kuhnert, P.M., 2015. Combining contemporary and long-term erosion rates to target erosion hot-spots in the Great Barrier Reef Australia. Anthropocene 10, 1–12.

Bierman, P.R., Steig, E.J., 1996. Estimating rates of denudation using cosmogenic isotope abundances in sediment. Earth Surf. Processes Landf. 21, 125–139.

Bierman, P.R., Reuter, J.M., Pavich, M.J., Gellis, A.C., Caffee, M.W., Larsen, J., 2005. Using cosmogenic nuclides to contrast rates of erosion and sediment yield in a semi-arid, arroyo-dominated landscape, Rio Puerco Basin, New Mexico. Earth Surf. Processes Landf. 30, 935–953.

Borchers, B., Marrero, S., Balco, G., Caffee, M., Goehring, B., Lifton, N., Nishiizumi, K., Phillips, F., Schaefer, J., Stone, J., 2016. Geological calibration of spallation production rates in the CRONUS-Earth project. Quat. Geochronol. 31, 188–198.

Brandt, J., Kuemmerle, T., Li, H., Ren, G., Zhu, J., Radeloff, V.C., 2012. Using Landsat imagery to map forest change in southwest China in response to the national logging ban and ecotourism development. Remote Sens. Environ. 121, 358–369.

Brown, L., Pavich, M.J., Hickman, R.E., Klein, J., Middleton, R., 1988. Erosion of the eastern United States observed with ^{10}Be. Earth Surf. Processes Landf. 13, 441–457.

Brown, E.T., Stallard, R.F., Larsen, M.C., Raisbeck, G.M., Yiou, F., 1995. Denudation rates determined from the accumulation of in-situ produced ^{10}Be in the Luquillo Experimental Forest Puerto Rico. Earth Planet. Sci. Lett. 129, 193–202.

Burchfiel, B.C., Chen, Z., 2012. Tectonics of the Southeastern Tibetan Plateau and Its Adjacent Foreland 210 The Geological Society of America, Boulder, CO.

Chappell, J., Zheng, H.B., Fifield, K., 2006. Yangtse River sediments and erosion rates from source to sink traced with cosmogenic Be-10: sediments from major rivers. Palaeogeogr. Palaeoclimatol. Palaeoecol. 241 (1), 79–94.

Chen, X., Lupi, F., He, G., Liu, J., 2009. Linking social norms to efficient conservation investment in payments for ecosystem services. Proc. Natl. Acad. Sci. 106 (28), 11812–11817. http://dx.doi.org/10.1073/pnas.0809980106.

Chen, J., Chen, J., Liao, A., Cao, X., Chen, L., He, C., Han, G., Peng, S., Lu, M., Zhang, W., Tong, X., Mills, J., 2015. Global land cover mapping at 30 m resolution: a POK-based operational approach. ISPRS J. Photogramm. Remote Sens. 103, 7–27.

Clapp, E.M., Bierman, P.R., Schick, A.P., Lekach, J., Enzel, Y., Caffee, M.W., 2000. Sediment yield exceeds sediment production in arid region drainage basins. Geology 28 (11), 995–998.

Clapp, E., Bierman, P.R., Caffee, M., 2002. Using ^{10}Be and ^{26}Al to determine sediment generation rates and identify sediment source areas in an arid region drainage basin. Geomorphology 45, 89–104.

Clift, P.D., 2006. Controls on the erosion of Cenozoic Asia and the flux of clastic sediment to the ocean. Earth Planet. Sci. Lett. 241 (3), 571–580.

Corbett, L.B., Bierman, P.R., Rood, D.H., 2016. An approach for optimizing *in situ* cosmogenic ^{10}Be sample preparation. Quat. Geochronol. 33, 24–34.

Costa, J.E., 1975. Effects of agriculture on erosion and sedimentation in piedmont province, maryland. Geol. Soc. Am. Bull. 86 (9), 1281–1286.

Covault, J.A., Romans, B.W., Graham, S.A., Fildani, A., Hilley, G.E., 2011. Terrestrial source to deep-sea sink sediment budgets at high and low sea levels: insights from tectonically active Southern California. Geology 39 (7), 619–622.

Covault, J.A., Craddock, W.H., Romans, B.W., Fildani, A., Gosai, M., 2013. Spatial and temporal variations in landscape evolution: historic and longer-term sediment flux through global catchments. J. Geol. 121 (1), 35–56.

Dadson, S., Hovius, N., Pegg, S., Dade, W.B., Horng, M.J., Chen, H., 2005. Hyperpycnal river flows from an active mountain belt. J. Geophys. Res. Earth Surf. 110 (F4). http://dx.doi.org/10.1029/2004JF000244.

Dixon, J.L., Heimsath, A.M., Amundson, R., 2009. The critical role of climate and saprolite weathering in landscape evolution. Earth Surf. Processes Landf. 11, 1507–1521.

Ferrier, K.L., Kirchner, J.W., Finkel, R.C., 2005. Erosion rates over millennial and decadal timescales at Caspar Creek and Redwood Creek, Northern California Coast Ranges. Earth Surf. Processes Landf. 30 (8), 1025–1038.

Gellis, A.C., Fuller, C.C., Van Metre, P.C., 2017. Sources and ages of fine-grained sediment to streams using fallout radionuclides in the Midwestern United States. J. Environ. Manage. 194, 73–85.

Gonzalez, V.S., Schmidt, A.H., Bierman, P.R., Rood, D.H., 2017. Spatial and temporal replicability of meteoric and *insitu* ^{10}Be concentrations in fluvial sediment. Earth Surf. Processes Landf. http://dx.doi.org/10.1002/esp.4205.

Graly, J.A., Reusser, L.J., Bierman, P.R., 2011. Short and long-term delivery rates of meteoric ^{10}Be to terrestrial soils. Earth Planet. Sci. Lett. 302 (3–4), 329–336. http://dx.doi.org/10.1016/j.epsl.2010.12.020.

Granger, D.E., Kirchner, J.W., Finkel, R.C., 1996. Spatially averaged long-term erosion rates measured from in-situ produced cosmogenic nuclides in alluvial sediment. J. Geol. 104, 249–257.
Henck, A.C., Montgomery, D.R., Huntington, K.W., Liang, C., 2010. Monsoon control of effective discharge, Yunnan and Tibet. Geology 38 (11), 975–978.
Henck, A.C., Huntington, K.W., Stone, J.O., Montgomery, D.R., Hallet, B., 2011. Spatial controls on erosion in the Three Rivers Region, southeastern Tibet and southwestern China. Earth Planet. Sci. Lett. 303, 71–83.
Hetzel, R., 2013. Active faulting, mountain growth, and erosion at the margins of the Tibetan Plateau constrained by in situ-produced cosmogenic nuclides. Tectonophysics 582, 1–24.
Hewawasam, T., Von Blanckenburg, F., Schaller, M., Kubik, P.W., 2003. Increase of human over natural erosion rates in tropical highlands constrained by cosmogenic nuclides. Geology 33 (7), 597–600.
Higgitt, D.L., Lu, X., 1996. Patterns of sediment yield in the Upper Yangtze basin, China. In: Walling, D.E., Webb, B.W. (Eds.), Erosion and Sediment Yield: Global and Regional Perspectivites, Volume IAHS Pub. No. 236. IAHS Press, Wallingford, Oxfordshire, pp. 205–214.
Jull, A.J.T., Scott, E.M., Bierman, P., 2015. The CRONUS-Earth inter-comparison for cosmogenic isotope analysis. Quat. Geochronol. 26, 3–10. http://dx.doi.org/10.1016/j.quageo.2013.09.003.
Kirby, E., Harkins, N., 2013. Distributed deformation around the eastern tip of the Kunlun fault. Int. J. Earth Sci. 102 (7), 1759–1772.
Kirchner, J.W., Finkel, R.C., Riebe, C.S., Granger, D.E., Clayton, J.L., King, J.G., Megahan, W.F., 2001. Mountain erosion over 10 yr, 10 ky., and 10 my. time scales. Geology 29 (7), 591–594.
Kohl, C.P., Nishiizumi, K., 1992. Chemical isolation of quartz for measurement of in-situ produced cosmogenic nuclides. Geochim. Cosmochim. Acta 56, 3583–3587.
Lal, D., Peters, B., 1967. Cosmic Ray Produced Radioactivity on the Earth. Springer, Berlin, pp. 551–612.
Lal, D., 1991. Cosmic ray labeling of erosion surfaces: *in situ* nuclide production rates and erosion models. Earth Planet. Sci. Lett. 104, 424–439.
Lal, R., 2003. Soil erosion and the global carbon budget. Environ. Int. 29 (4), 437–450.
Lu, X.X., Ashmore, P., Wang, J., 2003a. Sediment yield mapping in a large river basin: the Upper Yangtze, China. Environ. Model. Softw. 18 (4), 339–353.
Lu, X.X., Ashmore, P., Wang, J.F., 2003b. Seasonal water discharge and sediment load changes in the Upper Yangtze, China. Mt. Res. Dev. 23 (1), 56–64.
Lupker, M., Blard, P.H., Lave, J., France-Lanord, C., Leanni, L., Puchol, N., Charreau, J., Bourles, D., 2012. Be-10-derived Himalayan denudation rates and sediment budgets in the Ganga basin. Earth Planet. Sci. Lett. 333, 146–156.
Magee, D., 2006. Powershed politics: Yunnan hydropower under Great Western development. China Q. 185, 23–41.
Matmon, A., Bierman, P.R., Larsen, J., Southworth, S., Pavich, M.J., Finkel, R.C., Caffee, M.W., 2003. Erosion of an ancient mountain range, the Great Smoky Mountains, North Carolina and Tennessee. Am. J. Sci. 303, 517–855.
Matson, P.A., Parton, W.J., Power, A.G., Swift, M.J., 1997. Agricultural intensification and ecosystem properties. Science 277 (5325), 504–509.
Meyer, H., Hetzel, R., Fugenschuh, B., Strauss, H., 2010a. Determining the growth rate of topographic relief using in situ-produced Be-10: A case study in the Black Forest, Germany. Earth Planet. Sci. Lett. 290 (3), 391–402.
Meyer, H., Hetzel, R., Strauss, H., 2010b. Erosion rates on different timescales derived from cosmogenic 10Be and river loads: implications for landscape evolution in the Rhenish Massif, Germany. Int. J. Earth Sci. 99 (2), 395–412.
Milliman, J.D., Meade, R.H., 1983. World-wide delivery of river sediment to the oceans. J. Geol. 91 (1), 1–21.
Montgomery, D.R., 2007. Soil erosion and agricultural sustainability. Proc. Natl. Acad. Sci. U. S. A. 104 (33), 13268–13272.
NASA LP-DAAC, 2012. ASTER GDEM. NASA Land Processes Distributed Active Archive Center (LP DAAC). LP DAAC.
Nishiizumi, K., Imamura, M., Caffee, M.W., Southon, J.R., Finkel, R.C., McAninch, J., 2007. Absolute calibration of ^{10}Be AMS standards. Nuclear Instrum. Methods B 258 (2), 403–413.
Ouimet, W.B., Whipple, K.X., Granger, D.E., 2009. Beyond threshold hillslopes: channel adjustment to base-level fall in tectonically active mountain ranges. Geology 37 (7), 579–582.
Portenga, E.W., Bierman, P.R., 2011. Understanding earth's eroding surface with ^{10}Be. GSA Today 21 (8), 4–10. http://dx.doi.org/10.1130/g111a.1.
Portenga, E.W., Bierman, P.R., Duncan, C., Corbett, L.B., Kehrwald, N.M., Rood, D.H., 2015. Erosion rate of the Bhutanese Himalaya determined using in situ-produced ^{10}Be. Geomorphology 233, 112–126.
Regard, V., Carretier, S., Boeglin, J.L., Ndam Ngoupayou, J.R., Dzana, J.G., Bedimo Bedimo, J.P., Riotte, J., Braun, J.J., 2016. Denudation rates on cratonic landscapes: comparison between suspended and dissolved fluxes, and ^{10}Be analysis in the Nyong and Sanaga River basins, south Cameroon. Earth Surf. Processes Landf. 41 (12), 1671–1683. http://dx.doi.org/10.1002/esp.3939.
Reiners, P.W., Ehlers, T.A., Mitchell, S.G., Montgomery, D.R., 2003. Coupled spatial variations in precipitation and long-term erosion rates across the Washington Cascades. Nature 426 (6967), 645–647.
Reusser, L.J., Bierman, P.R., Rood, D.H., 2015. Quantifying human impacts on rates of erosion and sediment transport at a landscape scale. Geology 43 (2), 171–174.
Reusser, L.J., Bierman, P.R., Rizzo, D.M., Portenga, E.W., Rood, D.H., 2017. Characterizing landscape-scale erosion using ^{10}Be in detrital fluvial sediment: slope-based sampling strategy detects the effect of widespread dams. Water Resour. Res. 53 (5), 4476–4486. http://dx.doi.org/10.1002/2016WR019774.
Schäfer, J.M., Tschudi, S., Zhao, Z., Wu, X., Ivy-Ochs, S., Wieler, R., Baur, H., Kubik, P.W., Schlüchter, C., 2002. The limited influence of glaciations in Tibet on global climate over the past 170 000 yr. Earth Planet. Sci. Lett. 194 (3), 287–297.
Schaller, M., von Blanckenburg, F., Hovius, N., Kubik, P.W., 2001. Large-scale erosion rates from in situ-produced cosmogenic nuclides in European river sediments. Earth Planet. Sci. Lett. 188 (3), 441–458.
Schmidt, A.H., Montgomery, D.R., Huntington, K.W., Liang, C., 2011. The question of communist land degradation: new evidence from local erosion and basin-wide sediment yield in Southwest China and Southeast Tibet. Ann. Assoc. Am. Geogr. 101 (3), 1–20.
Schmidt, A.H., Neilson, T.B., Bierman, P.R., Rood, D.H., Ouimet, W.B., Sosa Gonzalez, V., 2016. Influence of topography and human activity on apparent *in situ* ^{10}Be-derived erosion rates in Yunnan, SW China. Earth Surf. Dyn. 4 (4), 819–830. http://dx.doi.org/10.5194/esurf-4-819-2016.
Shapiro, J., 2001. Mao's War Against Nature: Politics and the Environment in Revolutionary China. Cambridge University Press, Cambridge.
Siame, L.L., Angelier, J., Chen, R.F., Godard, V., Derrieux, F., Bourlès, D.L., Braucher, R., Chang, K.J., Chu, H.T., Lee, J.C., 2011. Erosion rates in an active orogen (NE-Taiwan): A confrontation of cosmogenic measurements with river suspended loads. Quat. Geochronol. 6 (2), 246–260. http://dx.doi.org/10.1016/j.quageo.2010.11.003.
Singleton, A.A., Schmidt, A.H., Bierman, P.R., Rood, D.H., Neilson, T.B., Greene, E.S., Bower, J.A., Perdrial, N., 2017. Effects of grain size, mineralogy, and acid-extractable grain coatings on the distribution of the fallout radionuclides ^{7}Be, ^{10}Be, ^{137}Cs, ^{210}Pb in river sediment. Geochim. Cosmochim. Acta 197, 71–86.
Stone, J., 1998. A rapid fusion method for separation of beryllium-10 from soils and silicates. Geochim. Cosmochim. Acta 62 (3), 555–561.
Stone, J.O., 2000. Air pressure and cosmogenic isotope production. J. Geophys. Res. 105 (B10), 23,573–523,579.
Summerfield, M., Hulton, N., 1994. Natural controls of fluvial denudation rates in major world drainage basins. J. Geophys. Res. Solid Earth 7, 13871–13883.
Syvitski, J.P.M., Vorosmarty, C.J., Kettner, A.J., Green, P., 2005. Impact of humans on the flux of terrestrial sediment to the global coastal ocean. Science 308 (5720), 376–380.
Trac, C.J., Harrell, S., Hinckley, T.M., Henck, A.C., 2007. Reforestation programs in Southwest China: reported success, observed failures, and the reasons why. J. Mt. Sci. 4 (4), 275–292. http://dx.doi.org/10.1007/s11629-007-0275-1.
Trac, C.J., Schmidt, A.H., Harrell, S., Hinckley, T.M., 2013. Is the returning farmland to forest program a success? Three case studies from Sichuan. Environ. Pract. 15 (3), 350–366.
Trimble, S.W., 1977. Fallacy of stream equilibrium in contemporary denudation studies. Am. J. Sci. 277 (7), 876–887.
Urgenson, L.S., Hagmann, R.K., Henck, A.C., Harrell, S., Hinckley, T.M., Shepler, S.J., Grub, B.L., Chi, P.M., 2010. Social-ecological resilience of a Nuosu community-linked watershed, southwest Sichuan, China. Ecol. Soc. 15 (4)(p. 2) http://www.ecologyandsociety.org/vol15/iss4/art2/.
Vanacker, V., Von Blanckenburg, F., Govers, G., Molina, A., Poesen, J., Deckers, J., Kubik, P., 2007. Restoring dense vegetation can slow mountain erosion to near natural benchmark levels. Geology 35 (4), 303–306.
Vanacker, V., Bellin, N., Molina, A., Kubik, P.W., 2014. Erosion regulation as a function of human disturbances to vegetation cover: a conceptual model. Landsc. Ecol. 29 (2), 293–309.
Vanmaercke, M., Poesen, J., Govers, G., Verstraeten, G., 2015. Quantifying human impacts on catchment sediment yield: a continental approach. Global Planet. Change 130, 22–36. http://dx.doi.org/10.1016/j.gloplacha.2015.04.001.
Von Blanckenburg, F., Hewawasam, T., Kubik, P.W., 2004. Cosmogenic nuclide evidence for low weathering and denudation in the wet, tropical highlands of Sri Lanka. J. Geophys. Res.: Earth Surf. 109 (F3), F03008. http://dx.doi.org/10.1029/2003JF000049.
Walling, D., Owens, P., Carter, J., Leeks, G., Lewis, S., Meharg, A., Wright, J., 2003. Storage of sediment-associated nutrients and contaminants in river channel and floodplain systems. Appl. Geochem. 18 (2), 195–220.
Walter, R.C., Merritts, D.J., 2008. Natural streams and the legacy of water-powered mills. Science 5861, 299–304.
Wang, G., Wu, B., Wang, Z.Y., 2005. Sedimentation problems and management strategies of Sanmenxia reservoir, Yellow River, China. Water Resour. Res. 41 (9), W09417.
Warrick, J.A., Farnsworth, K.L., 2009. Sources of sediment to the coastal waters of the Southern California Bight. Geol. Soc. Am. Spec. Pap. 454, 39–52.
Willenbring, J.K., von Blanckenburg, F., 2010. Meteoric cosmogenic Beryllium-10 adsorbed to river sediment and soil: applications for Earth-surface dynamics. Earth Sci. Rev. 98 (1–2), 105–122. http://dx.doi.org/10.1016/j.earscirev.2009.10.008.
Willett, S.D., Brandon, M.T., 2002. On steady states in mountain belts. Geology 30 (2), 175–178.
Wittmann, H., von Blanckenburg, F., 2009. Cosmogenic nuclide budgetng of floodplain sediment transfer. Geomorphology 109, 246–256.
Wittmann, H., von Blanckenburg, F., Guyot, J.L., Maurice, L., Kubik, P.W., 2009. From source to sink: preserving the cosmogenic ^{10}Be-derived denudation rate signal of the Bolivian Andes in sediment of the Beni and Mamoré foreland basins. Earth Planet. Sci. Lett. 288, 463–474.
Wittmann, H., von Blanckenburg, F., Maurice, L., Guyot, J.L., Filizola, N., Kubik, P.W., 2011. Sediment production and delivery in the Amazon River basin quantified by *in situ*-produced cosmogenic nuclides and recent river loads. Geol. Soc. Am. Bull. 123 (5–6), 934–950. http://dx.doi.org/10.1130/b30317.1.
Wittmann, H., Von Blanckenburg, F., Bouchez, J., Dannhaus, N., Naumann, R., Christl, M., Gaillardet, J., 2012. The dependence of meteoric 10Be concentrations on particle size in Amazon River bed sediment and the extraction of reactive 10Be/9Be ratios. Chem. Geol. 318–319, 126–138. http://dx.doi.org/10.1016/j.chemgeo.2012.04.031.
Xu, S., Freeman, S.P.H.T., Rood, D.H., Shanks, R.P., 2015. Decadal Be-10, Al-26 and Cl-36 QA measurements on the SUERC 5 MV accelerator mass spectrometer. Nucl. Instrum. Methods Phys. Res. Sect. B-Beam Interact. Mater. Atoms 361, 39–42.

Yang, Z.S., Yang, L.F., Zhang, B.S., 2010. Soil erosion and its basic characteristics at Karst Rocky-desertified land consolidation area: a case study at Muzhe Village of Xichou County in Southeast Yunnan, China. J. Mt. Sci. 7 (1), 55–72.

Yatagai, A., Kamiguchi, K., Arakawa, O., Hamada, A., Yasutomi, N., Kitoh, A., 2012. APHRODITE: Constructing a long-term daily gridded precipitation dataset for Asia based on a dense network of rain gauges. Bull. Am. Meteorol. Soc. 39 (9), 1401–1415.

Zhang, J., Pham, T., Kalacska, M., Turner, S., 2014. Using Landsat Thematic Mapper records to map land cover change and the impacts of reforestation programmes in the borderlands of southeast Yunnan, China: 1990–2010. Int. J. Appl. Earth Obs. Geoinf. 31, 25–36.